

Surface wave climatology and its variability in the North Indian Ocean based on ERA-Interim reanalysis

T.R. Anoop, V. Sanil Kumar*, P.R. Shanas, Glejin Johnson

Ocean Engineering, CSIR-National Institute of Oceanography (Council of Scientific & Industrial Research), Dona Paula, Goa 403 004 India

*Corresponding author: Tel: 0091 832 2450 327 Fax: 0091 832 2450 602 Email: sanil@nio.org

Abstract

The climate over the North Indian Ocean (NIO) is one of the most dynamic in the world due to seasonally reversing monsoon winds. In this study, we analyze the climate of the NIO and the variability of its surface waves using the European Centre for Medium Range Weather Forecast (ECMWF) global atmospheric re-analysis product (ERA-Interim) for the period 1979-2012. Annual average significant wave height (SWH) of NIO ranges from 1.5 to 2.5 m and the seasonal average is highest (3 to 3.5 m) during the monsoon (JJAS). Swells propagating from the southern hemisphere are present in the NIO during the pre-monsoon (FMAM) and post-monsoon (ONDJ). We separate the waves into wind seas and swells based on the wave energy statistical method. The results show that the NIO is swell-dominated and that wind sea heights are lower compared to the swell heights. Higher wind sea and swell heights are observed during the monsoon in the western NIO due to strong cross-equatorial winds of the Somali (Findlater) Jet. In the post-monsoon period, the eastern NIO shows a higher swell height than the western NIO shows. SWH shows an annual increasing trend in the western NIO. On a seasonal scale, the trends are increasing significantly in the monsoon compared to the post-monsoon period in a major part of the NIO, whereas the pre-monsoon period shows a decline in SWH. In NIO, monsoon is the dominant mode of variability and it covers 92 % of the total variability. Wave climate is also influenced by the annual and inter-annual variability in monsoon wind and rainfall.

Key words: surface waves, wave climate, long-term changes, monsoons, North Indian Ocean, inter-annual variability

1. Introduction

Climate change, a topic that is widely discussed worldwide, certainly has an impact on the oceans. The Indian Ocean is the third largest ocean in the world and covers approximately 20% of the water on the earth's surface (Rais 1987). The northern hemisphere of this basin, the North Indian Ocean (NIO), has a large influence on the scientific, industrial, engineering and commercial grounds of the countries on its rim. The NIO has a decisive role in the climate of the countries surrounding it and influences the rainfall of the densely populated coastal areas of south Asia (Clark *et al.* 2000). The unique geography of the NIO (Figure 1), being bounded to the north by the Asian continent, leads to a complex annual cycle associated with substantial seasonal reversals of the annual monsoon winds (Slingo *et al.* 2005). Wind waves are the prominent feature of the ocean surface and play a major role in planning activities in the open ocean and in coastal zones. Hence, a change in wave climate influences coastal and offshore activities. Waves in the NIO undergo large seasonal variations [monsoon (JJAS), pre-monsoon (FMAM) and post-monsoon (ONDJ)] due to the reversal of the large-scale wind field over the NIO between the boreal summer and winter (Kumar *et al.* 2012). The Indian subcontinent divides the NIO into two semi-enclosed seas: the Arabian Sea (AS) and the Bay of Bengal (BoB). Both of these seas encroach onto the equatorial regime of the basin (Shankar and Shetye 2001). The NIO, particularly the BoB region, is an area generally prone to cyclone events, and these events can result in large inter-annual variations in wave parameters.

Many regional studies have been conducted on the change in wave climate, especially in the North Pacific and North Atlantic regions (Carter and Draper 1988; Allan and Komar 2000; Caires and Swail 2004; Gulev and Grigorieva 2004; Parise and Farina 2012; Vanem and Walker 2013). Simmonds and Keay (2002) observed that the increase in wave height in the North Atlantic and North Pacific is due to the increase in cyclone numbers and the corresponding increase in the mean rate of mechanical energy input into the oceans. Vethamony *et al.* (2000) studied the wave climate of the Indian Ocean using altimeter and model data for the period 1986-1989. Young (1999) studied the seasonal variability of the global ocean wind and wave climatology based on a data set spanning a period of 10 years obtained from a combination of satellite remote sensing and model predictions. Based on the satellite altimeter and scatterometer data, Chen *et al.* (2002) presented swell and wind sea climate over the global ocean. As a part of the global study, Young *et al.* (2011) examined long-term trends in significant wave height (SWH) in the NIO from 1985-2008 based on satellite altimeter data. Semedo *et al.* (2011) presented a global view of the wind sea, and swell climate and variability based on the 45-yr European Centre for

Medium-Range Weather Forecast (ECMWF) wave reanalysis product (ERA-40). Sajiv *et al.* (2012) studied variations in wave characteristics during a 3-year period at a shallow water location in the eastern AS, and Shanas and Kumar (2014a) examined changes in wind speed and SWH at this location for 34 years. Using altimeter data, Kumar *et al.* (2013) studied changes in SWH and wind speed over the Indian Ocean for the period 1993-2010 by categorizing the area into six zones. Recently, Shanas and Kumar (2014b) analyzed trends in surface wind speed and SWH in the Central BoB. However, in these studies, the wave climatology and the long-term variations for the entire NIO are not well documented, and the need remains for a detailed analysis of the regional wave climate of the NIO. Hence, we analyze the wave climate of the NIO and its variability over different seasons and years.

2. Data and method

The present study is based on the global atmospheric reanalysis product of the ECMWF known as ERA-Interim (Dee *et al.* 2011). ERA-Interim is the latest global reanalysis product of ECMWF and is available from 1979 onwards. Based on an improved atmospheric model and assimilation procedures used in ERA-40, ERA-Interim uses a two-way coupled atmosphere–wave model system. The wave model (WAM) has also received some improvements, including a revised formulation of the ocean wave dissipation scheme and the introduction of a new scheme to parameterize unresolved bathymetry (Bidlot *et al.* 2007). A four-dimensional variational data assimilation scheme is used in ERA-Interim.

Kumar *et al.* (2013) compared wind stress estimates from ERA-Interim against in-situ observations in the tropical Indian Ocean and found that the data captured good temporal variability with better performance than other reanalysis data (the correlation coefficient was ~ 0.86). In the shallow waters of the eastern AS, Shanas and Kumar (2014a) found that ERA-Interim SWH data showed good correspondence with the measured wave rider buoy data. For the central BoB, Shanas and Kumar (2014b) found that ERA-Interim SWH data compared well with buoy data for mean values, but that ERA-Interim data under-predicted the measured SWH data up to 15% for high waves ($\text{SWH} > 2.5$ m). Durrant *et al.* (2013) found that a negative bias in modeled SWH has its origins primarily in the forcing; however, the reduction of systematic wind biases does not result in universal improvement in modeled SWH. In the present study, we use 34-year data (1979- 2012) of SWH at 6-h temporal and $1^\circ \times 1^\circ$ spatial resolutions. We also use ERA-Interim wind speed at a 10 m height of the same temporal and spatial resolution to separate waves into wind seas and swells.

Generally, the sea state is either wind seas dominated or swells dominated. We carry out the separation of wind seas and swells using wind speed and SWH based on the method proposed by Chen *et al.*

(2002). If U is the surface wind speed at 10 m above the sea surface, then the wind wave relation for a fully developed sea is (Chen *et al.* 1991),

$$SWH = 1.614 \times 10^{-2} U^2 \quad \text{for } 0 \leq U < 7.5 \text{ m s}^{-1} \quad (1)$$

$$SWH = 10^{-2} U^2 + 8.134 \times 10^{-4} U^3 \quad \text{for } 7.5 \leq U < 50 \text{ m s}^{-1} \quad (2)$$

Chen *et al.* (2002) introduced two probability indices for quantifying the frequency of occurrence of swell and wind seas: $P_s = N_s / N$ and $P_w = N_w / N$, where N_s and N_w are the numbers of swell dominated and wind sea dominated events at the study area, $N = N_s + N_w$, and P_s and P_w are statistical descriptions of the proportion of swell and wind sea dominances. Using these statistical proportions, we can separate the wind sea and swell energy from the total energy of the sea state based on the method suggested by Jiang and Chen (2013). The equations for estimating wind sea height (H_w) and swell height (H_s) from SWH are:

$$H_w = SWH \sqrt{P_w} \quad (3)$$

$$H_s = SWH \sqrt{P_s} \quad (4)$$

The assumptions are not strict and the statistical method does not work well for studies of short duration (such as 1 day). However, this method is helpful in obtaining a view of the wind sea and swell climatology.

Monthly average rainfall data provided by IITM (Indian Institute of Tropical Meteorology) obtained from rain gauges in various part of India from 1979 to 2012 is also used in the study (available at http://www.tropmet.res.in/static_page.php?page_id=53). We obtain the wave climate trend based on the slope of the linear best-fit curve to the annual mean SWH and the seasonal mean SWH for 34 years. The statistical significance of trends in the SWH is estimated by applying Kendall's Tau-Sen test (Sen 1968; Burkey 2006; <http://www.mathworks.com/matlabcentral/fileexchange>). Empirical orthogonal function (EOF), wavelet and cross wavelet methods (Torrence *et al.* 1998; Grinsted *et al.* 2004) are used to analyze the SWH, wind speed and rainfall data.

In order to know how the wave height is influenced by the tropical cyclone (TC), we have considered the TC events in AS for the period 1979-2012 using the position and intensity estimates reported in the JTWC best-track dataset (Chu *et al.* 2012). Classified the TC in different category; i) tropical depressions to cyclonic storms (wind speed \sim 17-47 knots), ii) severe cyclone category (wind speed \sim 48-63 knots) and iii) very severe cyclonic storms to super cyclones (wind speed $>$ 64 knots). Also we

analyzed the distribution of the locations where maximum intensity of TC observed and finally considered a box of latitude 17.5-22.5⁰N and longitude 60-65⁰E (Box A in Figure 1) to analyze the link between the severe cyclone events and SWH.

3. Results

3.1 Wave climatology of the North Indian Ocean

3.1.1 Significant wave height climatology

Figure 2 displays the annual mean SWH of the NIO and three seasonal SWH means. The range of the annual average SWH in the deep waters of the NIO is within 1.5 to 2.5 m (Figure 2a). The annual average SWH is higher (~ 2-2.5 m) off the south east coast of Sri Lanka, the west side of the Andaman and Nicobar Islands and the northeast coast of Africa. The annual average SWH in the coastal regions of the west and northeast coasts of India is 1 to 1.5 m. However, the annual average SWH is less than 1 m in the coastal region of the southeast coast of India due to the sheltering effect of the Sri Lankan land mass.

The seasonal climatology of the SWH in the pre-monsoon period indicates that the waves over the NIO become low in height due to a lower wind speed over the basin. The NIO is calm with a SWH ranging from 0.5 to 1.5 m (Figure 2b). During this time, the southwestern and southeastern NIO show higher SWHs compared to other regions. The SWH is decreasing from south to north and southwest to northeast in the eastern and western NIO respectively. During the Asian summer monsoon, due to the strong cross-equatorial winds of the Findlater (Somali) Jet (Findlater 1969), wave heights are high in the AS. Consequently, the maximum average wave height (3 to 3.5 m) for the NIO during monsoon season occurs in the western AS as a result of the strong southwesterly winds caused by the East African highlands (Slingo *et al.* 2005). These southwesterly winds spread and wane in the northeast direction (Slingo *et al.* 2005), as do the waves (Figure 2c). Hence, high waves reach the northern part of the west coast of India before they reach the southern part.

A study by Glejin *et al.* (2012) observed higher swells are present at the northern part of the NIO along the eastern AS compared to the southern part. The monsoon wind in the NIO splits into two branches from the southern part of the Indian sub-continent: (1) the AS branch and (2) the BoB branch. The monsoon winds in the BoB are weaker than the monsoon winds in the AS. The BoB branch generates surface waves in the southern BoB, but these waves do not reach the major part of the southeast coast due to the sheltering of the Sri Lankan island. The lower wave height in the western BoB, compared to

the wave height in the eastern AS during the monsoon season, is not only due to weaker BoB winds in the monsoon, but also due to the sheltering effect of Sri Lanka.

Semedo *et al.* (2011) noted that the SWH seasonal mean maxima in the Southern Hemisphere are located in the Southern Ocean Indian sector. Extreme wave conditions occur at high southern latitudes due to the massive amounts of kinetic energy deposited into the Southern Ocean associated particularly with the transient meteorological systems (Simmonds *et al.* 2005). Young (1999) discussed the important role played by the intense wave generation systems of the Southern Ocean and confirmed it to be consistently the roughest ocean on earth. Alves (2006) reported that the waves generated along the Southern Ocean storm belt have a considerable impact on the global wave climate due to swell propagation. The wave height in the NIO during the post-monsoon period is higher than it is in the pre-monsoon. During the post-monsoon period, high waves (Figure 2d) are observed in the southern NIO with a maximum SWH (~ 2-2.5 m) in the BoB rather than in the AS (~ 1.5-2 m) due to the closure effect of the Maldives land mass to the Southern Ocean swells. Due to northeast monsoon winds, the wave height in the BoB is higher than that in the AS during the post-monsoon period (Glejin *et al.* 2013).

Spatial distribution of yearly and seasonal standard deviation (SD) of SWH from 1979 to 2012 is shown in the right panel of Figure 2. The annual SD shows that it is less than 0.05 m in most of the region (Figure 2e). Annual SD maximum is 0.07 m in western AS at northeast coast of Africa and it spread towards north through western NIO. During pre-monsoon SD is less than 0.1 m in most of the region and higher values are observed in the south western region of AS (Figure 2f). In NIO, higher SD is observed during monsoon compared to other seasons (Figure 2g). During this period, the western and northern AS shows higher SD with northern AS as slightly higher value (~ 0.16 m) than western AS. During this time the BoB region also shows higher value (~ 0.11 m) compared to other seasons, but even during monsoon, the south to central east coast of India shows very small SD. This low SD could be due to the sheltering effect of Sri Lankan land mass. The Sri Lankan land mass has a major role in the wave climate of major part of eastern shelf seas of India. In post-monsoon season the higher SD is observed in southeast of NIO and western AS (Figure 2h).

3.1.2 Swell and wind sea climatology

The annual and seasonal climatology of wind seas and swells in the NIO are shown in Figure 3. It is clear from left panel of Figure 3 that swell SWH is always higher than wind sea SWH (right panel of Figure 3). The annual climatology of wind seas and swells indicates that the waves in NIO are dominated by swells (Figure 3a). The annual average of the wind sea height is less than 1 m in major

part of the NIO. Wind sea height of more than 1 m is observed in the south at the eastern entrance of the Gulf of Aden (off the northeast coast of Africa). In seasonal climatology, wind seas are very low during the pre-monsoon season (Figure 3b). During this time, swells are in the range of 1 to 1.5 m and swell height decreases from south to north in the NIO. Semedo *et al.* (2011) and Glejin *et al.* (2013b) found that the swell propagating from the southern hemisphere reaches the west coast of India during the pre-monsoon period. Due to the calm condition (low wind seas) of the NIO during the pre-monsoon period, the propagation of swells from the southern hemisphere is more visible. These swells are absent during the monsoon season due to turbulence in the NIO created by strong winds (Glejin *et al.* 2013b). Chen *et al.* (2002) observed an enhancement of the wind sea generation in the AS in the boreal summer (JJA) as a consequence of the Asian monsoon. Semedo *et al.* (2011) also reported that the NIO, with the exception of the summer monsoon period (JJA), is the most swell-dominated area of the World Oceans. In the eastern AS, the average period of swells in the monsoon is less than that during the other two seasons (Kumar *et al.* 2012) because these swells are generated within the western NIO (Figure 3c) and reach the west coast of India from a southwest direction. The swells in the western NIO are due to a higher southwest wind condition in this region (average wind speed ~ 11 to 12 m s^{-1}). Due to this higher wind speed, a wind sea height greater than 2 m is observed only during the monsoon season in the western NIO. Higher winds in this region pump energy mostly into shorter (high frequency), slowly moving waves. These waves transfer this energy across the continuous spectrum of waves of all scales towards longer (lower frequency) components, thus allowing the longer (lower frequency) waves to grow by means of non-linear interaction (Babanin 2011). The generated swells reach the west coast of India.

In the BoB region, the southern BoB shows a higher swell height than other regions due to the propagation of swells from the South Indian Ocean. Chen *et al.* (2002) identified the southern BoB as one of the major swell pools in the world's oceans. A surface wind speed (not shown) that is higher during the post-monsoon period than in pre-monsoon period generates relatively high waves in the NIO during the post-monsoon (Figure 3d). During this period, comparatively higher swell and wind sea heights are observed on the northeastern coast of Africa, but this wave system is weak during the pre-monsoon season. Glejin *et al.* (2013b) observed that waves with peak wave period 8 to 13 s reaches the central west coast of India during the post-monsoon period from southwest direction, whereas the occurrence of these waves is much less during the pre-monsoon season.

3.2 Variability of wave height

3.2.1 Wave trend analysis

The yearly and seasonal trends of SWH in the NIO are shown in Figure 4. Compared to the seasonal cycle, the linear trend in the SWH is relatively small. Trend of SWH with significance level greater than 90% is only shown in Figure 4. The western part of the NIO shows a yearly increasing trend (Figure 4a), and in this region, the eastern entrance of the Gulf of Aden and the western equatorial Indian Ocean shows the maximum value ($\sim 0.4 \text{ cm yr}^{-1}$). The western Indian Ocean shows an increasing wave height at the rate of 0.1 to 0.4 cm yr^{-1} . The SWH in the waters of two semi-enclosed basins, the Red Sea and the Persian Gulf, also shows this increasing trend. These regions are important for the transport of cargo vessels carrying oils and goods. Hence, an increase in wave height can affect marine transport in this region. In a small area near the east coast of India, a decreasing trend of SWH is observed.

We compared our estimated SWH trend with that reported by Young *et al.* (2011). Young *et al.* (2011) reported that the long-term trend of SWH in the NIO was in the range of 0 to 0.75% (0 to 0.75 cm yr^{-1}) during the period 1985-2008. During the same period, the present study shows a similar increasing trend in most of the regions. Some parts of the NIO show a decreasing trend similar to the trend observed in Young *et al.* (2011), but regionally, a slight difference is observed in both studies. For example, our study shows a decreasing trend in small area of central east coast of India whereas, the study of Young *et al.* (2011) show small increasing trend in that region.

Two transects of width 10° of longitude and centred on 65.25 and 90°E were calculated from 53.25°S to 20.25°N , with a view to examining the annual mean SWH trends in Indian Ocean. The trend of SWH decreases from south to north along both transects (0.86 to 0.04 cm y^{-1} along 65.25°E and from 0.79 to -0.05 cm y^{-1} along 90°E) except at the northern most location. The northern location at both transects indicated a higher increasing trend (Figure 5). Statistical significance levels of the trends at locations 1, 4, 5, 7, 11 to 14 are above 95%, at locations 6, 8 and 10 are above 90%, at location 3 is above 86% and at locations 2 and 9 are insignificant. Since the waves in the eastern AS are mainly the swells arriving from Southern Ocean (Semedo *et al.* 2011; Glejin *et al.* 2013b), the increase in SWH in NIO is due to the increase in swells in the Southern Ocean. Hemer *et al.* (2008) reported that the wave events are likely to increase in magnitude in the southern coast of Australia due to intensification of the storms. Hemer *et al.* (2010) observed increasing trend in SWH for Indian Ocean sector of Southern Ocean.

During pre-monsoon, a large area in the northeastern AS, northwestern BoB and southern region of the AS shows a decreasing SWH (Figure 4b). The region near the Andaman and Nicobar Islands also shows a decreasing SWH. However, during monsoon, the SWH shows a strong increasing trend in almost all areas (Figure 4c). It has increased more than 1 cm yr^{-1} in the northern AS and is at the highest value this season. The second maximum is observed in the western equatorial Indian Ocean. During this season, the eastern NIO and the northern BoB show an increasing trend. In the post-monsoon season, a strong increasing trend in SWH is observed in the southwestern NIO (Figure 4d). A greater increasing trend is observed in the eastern entrance of the Gulf of Aden ($> 0.5 \text{ cm yr}^{-1}$). The region around Sri Lanka (the southern region of the Indian subcontinent) shows an increasing SWH in the range of 0.2 to 0.3 cm yr^{-1} .

To explore the influence of local winds on the waves, the trend of wind speed is examined (Figure 4e-h). Western AS shows a positive trend in wind speed similar to the trend of SWH. Similar to the observation of Shanas and Kumar (2014a) annual mean wind speed shows a statistically significant decreasing trend of 1-2 cm/s/year in the central eastern AS.

3.2.2 Modes of variability of SWH

The empirical orthogonal function (EOF) method is used in this section to represent different modes of variability of SWH in NIO. We have carried out the analysis using the monthly average SWH and wind speed. The first EOF mode of SWH (EOF1 (SWH)) covers 92% of total variability in NIO (Figure 6a) and all other modes are degenerate ($\sim 8\%$). EOF1 (SWH) exhibits maximum value at the west of the study area and it mainly spread and wane towards the north and northeast. Weak branch of it enters the BoB through the southern part of India. The first mode of variability of wind speed is shown in Figure 6b and it covers 70% of the total variability. Since the waves are mainly generated in the ocean surface by the wind stress acting on water and this stress is directly proportional to the square of wind speed, the climatology of square of wind speed for the monsoon months from 1979 to 2012 is presented in Figure 6d. Figures 6a and 6b show same pattern of Figure 6d and hence, we can say that first EOF mode of SWH and wind speed in NIO is due to the monsoon wind. The BoB branch of monsoon is also visible in these figures.

The correlation of principal component time series of SWH (PC1 (SWH)) and that of wind speed (PC1 (WS)) are 0.94 with significance level above 95%. The PC1 (SWH) and PC1 (WS) are shown in Figure 6c which shows the annual oscillation of monsoon. From the above factors, it is clear that the wave climate variability in NIO is influenced by the monsoon wind. Modes of monthly anomaly of SWH are shown in Figure 6e. From the figure it is clear that strong negative variability in AS is similar to the

EOF1 of SWH and wind speed. It is spreading and waning to northwest direction. The EOF1 of SWH anomaly covers 51% percentage of total variability of SWH anomaly in NIO. The PC1 of first mode of SWH and wind speed anomaly are shown in Figure 6f. The correlation between wind speed and SWH is 0.54 with significance level greater than 99%. From the time series of EOF1 of SWH anomaly (Figure 6f), it can be seen that some extreme events during the monsoon period occur from 1979 to 2012.

To identify the influence of inter-annual variability of monsoon on NIO wave climate, we used the PC1 (SWH) and that of wind speed with monthly average rainfall data for central west coast of India (Goa and Konkan region) and all India. In the case of central west coast of India, the annual rainfall is predominantly during the monsoon. For all India rainfall data, the monsoon contributes 60 to 90% of annual rainfall (Rameshkumar *et al.* 2004). The yearly oscillation of monsoon and wave climate is well known so that in this study we focused on the inter-annual oscillation of monsoon and its relation to SWH. Here, we selected one box in central AS (10 to 15 °N and 60 to 65 °E, Box B in Figure 1), where higher variability of SWH is observed in EOF1 (SWH). Correlation of monthly and spatially averaged SWH over Box B in central AS (Figure 1) with the rainfall over the central west coast and all over the India are high (correlation coefficient of 0.93 and 0.91 respectively; both are statistically significant at 99%). Time series plot of monsoon mean SWH and wind speed within the Box B at central AS and monthly average rainfall data during monsoon in central west coast of India indicate that in some years the increase/decrease in SWH is linked to rainfall (Figure 7). But in some years (e.g. 1986, 1994, 2001 and 2012) even though the SWH was high similar increase in rainfall was not observed and also when the rainfall was high, lower SWH is observed in some years (e.g. 1985, 1987, 1997, 2000 and 2011). Whereas the monsoon mean SWH has a correlation with the monsoon mean wind speed (correlation coefficient 0.77). The study shows that simple correlation or lag correlation analysis is insufficient for understanding the influence of inter-annual oscillations of monsoon on SWH.

To remove the oscillations in period range of one year and less than one year, the time series data is low pass filtered using butterworth filter. This filtered and non-filtered data is analyzed with wavelet and wavelet coherence analysis (Torrence *et al.* 1998; Grinsted *et al.* 2004) and shown in Figures 8 and 9 respectively. In the case of SWH, we can see two bands of oscillations; one in the 4 to 6 year band and the other one in 7 to 10 year band (Figure 8a). Among these two bands, the 7 to 10 year band is continuous, whereas 4 to 6 year band is observed till 1997 and after that it shifted gradually to 5 to 10 year band and became a combined one. Similar pattern of oscillations are observed in case of PC1 of surface wind (Figure 8b) and monthly average rainfall on central west coast (Figure 8c) of India and all

over India (Figure 8d) also. The rainfall data of central west coast region shows large similarity with PC1 of SWH than compared to all India rainfall, because the all India rainfall is influenced by the northeast monsoon (OND) also (Kripalani *et al.* 2004).

By separating the modes of SWH using EOF, we found that the monsoon covers 92 % as first mode of variability. The phase relation between the SWH within the Box B (Figure 1) and rainfall in central west coast of India (monsoon rainfall) is identified with help of cross wavelet coherence analysis (Grinsted *et al.* 2004). Figure 9 shows cross wavelet of SWH in spatial and monthly averaged within the box with monthly rainfall in central west coast of India. From the figure, it is clearly visible that the SWH and monsoon rainfall is related with phase angle 0° indicating that in a yearly cycle, both of them are in phase. In case of inter-annual cycle we already discussed about two bands of oscillation which was observed from filtered data and this band is also visible here. Among this phase angle, 7 to 10 year band is 0° as one year band, but phase angle 50° is observed in the case of 4 to 6 year band up to the year 1997. The 50° upward phase angle indicates that the monsoon rainfall leads SWH by 50° phase for this period.

3.3 Influence of Tropical cyclones on wave height over the NIO

A detailed climatology of tropical cyclones (TCs) in AS is reported by Evan and Camargo (2011). Evan *et al.* (2011) reported an increase in intensification of tropical cyclones during the pre-monsoon season. For the study period, we have observed around 60 TCs over the NIO of which i) 50% are observed as tropical depression to cyclonic storms (wind speed 17-47 knots), ii) 23 % comes under the severe cyclone category (wind speed 48-63 knots), and iii) 27% as very severe cyclonic storms to super cyclones (wind speed >64 knots) (Figure 10a).

If we consider the maximum intensity of TC during the whole study period, there is a clear intensification of stronger events after 1996 (Figure 10b). Evan *et al.* (2011) reported that the early development of the monsoon may be caused by enhanced land-ocean thermal contrast between the Asian landmass and the equatorial Indian Ocean, which can reinforce the northward pressure gradients that in turn strengthen the monsoon and associated cyclonic shear vorticity. We considered the distribution of the locations where maximum intensity of TC is observed in AS and found that the occurrences of stronger events such as severe cyclones and super cyclones of maximum intensity are mostly in the area covering $17.5-22.5^{\circ}\text{N}$ and $60-65^{\circ}\text{E}$. Hence, we have considered a box area (latitude $17.5-22.5^{\circ}\text{N}$ and longitude $60-65^{\circ}\text{E}$, Box A in Figure 1) to analyze the link between the severe cyclone events and SWH. The analysis showed about 16 cyclones passed through the box and out of which the

most severe events were selected for the study. The details of the cyclones date and their maximum intensity locations are presented in Table 1.

The selected cyclone events are during 1993, 2007 and 2010 and the strongest was the super cyclonic storm Gonu, which formed in early June 2007. We have extracted the time series data of SWH for each year at the location where the maximum cyclone intensity is observed. The encircled peaks in SWH (Figure 11b) in all three years are due to the cyclone activity and the SWH and wind speed observed during the maximum cyclone intensification for the study domain is presented in panel 3 and 4 of Figure 11. Increase in wind speed and associated wave height is observed all throughout the events. The unusual intensification of SWH is directly related to the TC activity. As the TC moves the local wind speed becomes higher, which could generate higher wind seas. About 90% of the pre-monsoon TC in AS occurs from mid-May to mid-June, during which the mean vertical wind shear over the TC intensification zone increases approximately from 12 m s^{-1} to 25 m s^{-1} (Evan *et al.* 2011). Evan *et al.* (2011) also reported that the lifetime maximum intensification date of TCs also increased during the recent decade to around 13 days confirmed with higher confidence level. Since the intensity of cyclones increased and are mostly occurred in latitude greater than 15° N the trend of SWH is higher in the north-eastern part of NIO (Figures 4a and 5).

4. Summary and conclusions

The climatology and variability of surface waves in the NIO region is investigated using ERA-interim reanalysis data. This study focuses on the period 1979-2012 and includes the analysis of significant wave height, swell and wind sea height. Wind sea and swells are separated from the wave data using the wave energy statistical method. The variability of the SWH for 34 years is studied by trend analysis and EOF analysis and role of tropical cyclones on the SWH variability are also examined. In the trend analysis, the western NIO shows a strong increasing trend and the increase in wave height in this area can affect the eastern coastal region of Africa. A higher annual increasing is observed in the western equatorial NIO and east of the eastern entrance of the Gulf of Aden. An annual decreasing SWH is observed in a small area along the east coast of India. During the pre-monsoon period, the NIO is relatively calm and shows a decreasing trend in SWH. A higher increasing SWH is observed during the monsoon season. The northern NIO shows an increasing trend of greater than 1 cm yr^{-1} . The swells from the southern hemisphere are present in the NIO during the pre and post-monsoon seasons. The increasing and decreasing SWH in NIO depends on the southern hemispheric swells and local wind system. The intermediate period waves generated off the northeast coast of Africa are propagated in a

northeast direction and are observed in the eastern Arabian Sea. The EOF analysis indicates that the SWH variance is strongly dominated by the first mode and is associated with the monsoon wind in the NIO. A higher variability in the SWH is observed in the western AS region and is spreading and waning in the northeast direction. The unusual intensification SWH in NIO is directly related to the tropical cyclone activity. And also there is a clear intensification of stronger events after 1996. Since the intensity of cyclones are increasing it will have much influence on the seasonal characteristics of SWH of the region. Wave climatology and trends in the NIO require further investigation in order to determine the role of the Southern Ocean swell in their modulation and the influence of inter-annual variation in monsoon on SWH.

Acknowledgements

We thank the Director of the CSIR-National Institute of Oceanography, Goa for providing encouragement in carrying out the study. We thank Indian Institute of Tropical Meteorology, Pune, India for providing the rainfall data. We thank the two reviewers for their critical comments and the suggestions for additional studies which improved the scientific content of the paper. This work forms part of the Ph.D. thesis of the first author. This work is the NIO contribution No. xxxx.

References

- Allan, J., and P. D. Komar, 2000: Are ocean wave heights increasing in the eastern North Pacific? *Eos Trans. AGU*, **47**, 566–567.
- Alves, J. H. G. M., 2006: Numerical modeling of ocean swell contributions to the global wind-wave climate. *Ocean Modell.*, **11**, 98–122.
- Babanin, A. V., 2011: Breaking and dissipation of ocean surface waves, Cambridge University Press, Cambridge , 463pp.
- Bidlot, J. R., P. Janssen, and S. Abdalla, 2007: A revised formulation of ocean wave dissipation and its model impact. ECMWF Tech. Memo. 509, ECMWF, Reading, United Kingdom, 27 pp. [Available online at [http://www.ecmwf.int/publications/.](http://www.ecmwf.int/publications/)]
- Burkey, J., 2006: A non-parametric monotonic trend test computing Mann-Kendall Tau, Tau-b, and Sen's Slope written in Mathworks-MATLAB implemented using matrix rotations, King County, Department of Natural Resources and Parks, Science and Technical Services section, Seattle, Washington, USA.

Caires, S. and V. Swail, 2004: Global wave climate trend and variability analysis. Proceeding of the 5th International Workshop on Wave Hindcasting and Forecasting. Oahu, HI. U.S. Army Engineer Research and Development Center's Coastal and Hydraulics Laboratory and Cosponsors. CD-ROM. Al.

Carter, D. J. T., and L. Draper, 1988: Has the North East Atlantic become rougher? *Nature*, **332**, 494.

Chen, G., B. Chapron, R. Ezraty, and D. Vandemark, 2002: A global view of swell and wind sea climate in the ocean by satellite altimeter and scatterometer. *J. Atmos. Oceanic Technol.*, **19**, 1849–1859.

Chu, J.H., A.S. Levine, S. Daida, D. Schiber, E. Fukada, C.R. Sampson, 2012. Best track archive – North Indian Ocean. Naval Research Lab, Monterey and JTWC. http://www.usno.navy.mil/NOOC/nmfcph/RSS/jtwc/best_tracks/ioindex.html (accessed 6 January 2013).

Clark, C. O., J. E. Cole, and P. J. Webster, 2000: Indian Ocean SST and Indian summer rainfall: Predictive relationships and their decadal variability. *J. Climate*, **13**, 2503–2519.

Dee, D.P., et al., 2011: The ERA-Interim reanalysis: Configuration and performance of the data assimilation system. *Q. J. R. Meteorolog. Soc.*, **137**, 553-597.

Durrant, T.H., D.J.M. Greenslade, and I. Simmonds, 2013: The effect of statistical wind corrections on global wave forecasts. *Ocean Modell.*, **70**, 116-131. doi:10.1016/j.ocemod.2012.10.006.

Evan, A. T. and S.J. Camargo, 2011: A climatology of Arabian Sea cyclonic storms. *J. Clim.* **24**, 140-158.

Evan, A. T., J.P. Kossin, C.E. Chung, and V. Ramanathan, 2011: Arabian Sea tropical cyclones intensified by emissions of black carbon and other aerosols. *Nature* **479**, 94-97.

Findlater, J., 1969: A major low-level air current near the Indian Ocean during the northern summer. *Quart. J. Roy. Meteor. Soc.*, **95**, 362-380, doi:10.1002/qj.49709540409.

Glejin J., V. S. Kumar, and T. M. B. Nair, 2013a: Monsoon and cyclone induced wave climate over the near shore waters off Puduchery, south western Bay of Bengal. *Ocean Eng.*, **72**, 277-286.

Glejin J., V. S. Kumar, S. Philip, J. Singh, P. K. Pednekar, A. Kumar, G. U. Dora, and R. Gowthaman, 2012: Variations in Swells along Eastern Arabian Sea during the Summer Monsoon. *Open J. Mar. Sci.*, **2**, 43-50.

Glejin J., V. S. Kumar, T. M. B. Nair, and J. Singh, 2013b: Influence of winds on temporally varying short and long period gravity waves in the near shore regions of the eastern Arabian Sea. *Ocean Sci.*, **9**, 343-353.

- Grinsted, A., J. C. Moore, and S. Jevrejeva, 2004: Application of the cross wavelet transform and wavelet coherence to geophysical time series, *Nonlin. Processes Geophys.*, **11**, 561–566, doi:10.5194/npg-11-561-2004.
- Gulev, S. K. and V. Grigorieva, 2004: Last century changes in ocean wind wave height from global visual wave data. *Geophys. Res. Lett.*, **31**, L24302,
- Hemer, M.A., I. Simmonds and K. Keay, 2008: A classification of wave generation characteristics during large wave events on the southern Australian margin. *Cont. Shelf Res.*, **28**, 634-652.
- Hemer, M.A., J.A. Church and J.R. Hunter, 2010: Variability and trends in the directional wave climate of the Southern Hemisphere. *Int. J. Climatol.*, **30**, 475–491.
- Jiang, H. and G. Chen, 2013: A Global View on the Swell and Wind Sea Climate by the Jason-1 Mission: A Revisit, *J. Atmos. Oceanic Technol.*, **30**(8), 1833-1841.
- Kripalani, R. H., and P. Kumar, 2004: Northeast monsoon rainfall variability over south peninsular India vis-à-vis the Indian Ocean dipole mode. *Int. J. Climatol.*, **24**(10), 1267-1282.
- Kumar, B. P., J. Vialard, M. Lengaigne, V. S. N. Murty, M. J. McPhaden, M. F. Cronin, F. Pinsard, and K. G. Reddy, 2013: TropFlux wind stresses over the tropical oceans: evaluation and comparison with other products. *Climate Dyn.*, 40, 2049-2071, doi: 10.1007/s00382-012-1455-4.
- Kumar, D., S. A. Sannasiraj, V. Sundar, and V. G. Polnikov, 2013: Wind Wave Characteristics and Climate Variability in the Indian Ocean Region Using Altimeter Data. *Mar. Geod.*, **36**, 303-313.
- Kumar, V. S., J. Glejin., G. U. Dora., C. P. Sajiv, J. Singh, and P. Pednekar, 2012: Variations in nearshore waves along Karnataka, west coast of India. *J. Earth Sys. Sci.*, **121**, 393–403.
- Parise, C. K. and L. Farina, 2012: Ocean wave modes in the South Atlantic by a short-scale simulation, *Tellus A*, **64A**, 17362, doi: 10.3402/tellusa.v64i0.17362.
- Rais, R.B., 1987: Indian Ocean and the superpowers. Barnes and Noble Books, New Jersey, ISBN 0-389-20695-4, 215 p.
- RameshKumar, M. R., and U.R. Prabhu Dessai, 2004: A new criterion for identifying breaks in monsoon conditions over the Indian subcontinent. *Geophys. Res. Lett.*, **31**(18), L18201, doi:10.1029/2004GL020562.
- Sajiv, P. C., V. S. Kumar, J. Glejin, D. G. Udhaba, and P. Vinayaraj, 2012: Interannual and seasonal variations in nearshore wave characteristics off Honnavar, west coast of India. *Curr. Sci.*, **103**, 286-292.
- Semedo, A., K. Sušelj, A. Rutgersson, and Sterl, A., 2011: A global view on the wind sea and swell climate and variability from ERA-40. *J. Clim.*, **24**(5), 1461-1479,

- Sen, P. K., 1968: Estimates of the regression coefficient based on Kendall's tau, *J. Amer. Statist. Assoc.*, **63**, 1379-1389.
- Shanas, P. R., and V. S. Kumar, 2014a: Temporal variations in the wind and wave climate at a location in the eastern Arabian Sea based on ERA-Interim reanalysis data. *Nat. Hazards Earth Syst. Sci.*, **14**, 1371–1381, doi:10.5194/nhessd-1-1-2013.
- Shanas, P. R., and V. S. Kumar, 2014b: Trends in surface wind speed and significant wave height as revealed by ERA-Interim wind wave hindcast in the Central Bay of Bengal, *Int. J. Climatol.*, doi: 10.1002/joc.4164.
- Shankar, D., and S. Shetye, 2001: Why is mean sea level along the Indian coast higher in the Bay of Bengal than in the Arabian Sea ? *Geophys. Res. Lett.*, **28**(4), 563–565.
- Simmonds, I., A. Rafter, T. Cowan, A.B. Watkins and K. Keay, 2005: Large-scale vertical momentum, kinetic energy and moisture fluxes in the Antarctic sea-ice region. *Boun.-Layer Meteor.*, 117, 149-177.
- Simmonds, I., and K. Keay, 2002: Surface fluxes of momentum and mechanical energy over the North Pacific and North Atlantic Oceans. *Meteor. Atmos. Phys.*, 80, 1-18.
- Slingo, J., H. Spencer, B. Hoskins, P. Berrisford, and E. Black, 2005: The meteorology of the Western Indian Ocean and the influence of the East African Highlands, *Phil. Trans. R. Soc. A* **363**, 25-42, doi: 10.1098/rsta.2004.1473.
- Torrence, C., and G.P. Compo, 1998: A practical guide to wavelet analysis, *Bull. Am. Meteorol. Soc.*, **79**, 61–78.
- Vanem, E., and S.-E. Walker, 2013: Identifying trends in the ocean wave climate by time series analyses of significant wave height data. *Ocean Eng.*, **61**, 148–160.
- Vethamony, P., L. V. G. Rao, R. Kumar, A. Sarkar, M. Mohan, K. Sudheesh, and S. B. Karthikeyan, 2000: Wave climatology of the Indian Ocean derived from altimetry and wave model. In Proceedings of PORSEC, V I 301–304, 5–8 Dec 2000, Goa, India.
- Young, I. R., 1999: Seasonal variability of the global ocean wind and wave climate. *Int. J. Climatol.*, **19**, 931–950.
- Young, I. R., S. Zieger, and A. Babanin, 2011: Global trends in wind speed and wave height. *Science*, **332**(6028), 451–455.

Figure captions

Figure 1. The map showing the area studied (North Indian Ocean). The shadings are the depth in m. Map is plotted using ocean data viewer. The area ($17.5\text{-}22.5^{\circ}$ N and $60\text{-}65^{\circ}$ E) to analyze the link between the severe cyclone events and SWH is shown as A. The area in AS ($10\text{-}15^{\circ}$ N and $60\text{-}65^{\circ}$ E) used to study the phase relation between the SWH and rainfall in central west coast of India is shown as B.

Figure 2. North Indian Ocean wave climatology based on data from 1979 to 2012. Left panel shows the mean significant wave height a) annual, b) pre-monsoon, c) monsoon and d) post-monsoon. Right panel shows the standard deviation of significant wave height in NIO; e) annual, f) pre-monsoon, g) monsoon and h) post-monsoon. All the values are in meter.

Figure 3. Mean swell (left panel) and wind sea (right panel) height in NIO by wave energy statistical method (a. Annual, b. Pre-monsoon (FMAM), c. Monsoon (JJAS) and d. Post-monsoon (ONDJ). All the values are in meter.

Figure 4. Left panel shows the trend of significant wave height (cm yr^{-1}) (a. Annual, b. Pre-monsoon, c. Monsoon, d. Post-monsoon). Right panel shows the trend of wind speed ($\text{m s}^{-1} \text{yr}^{-1}$) (e. Annual, f. Pre-monsoon, g. Monsoon, h. Post-monsoon). White patches in oceans indicate values which fail to achieve statistical significance. Statistical significance more than 90% only is presented in this figure.

Figure 5. Trend of annual mean SWH along two transects in Indian Ocean. The left panel is along 65.25° E and the right panel is along 90° E. Statistical significance levels of the trends at locations 1, 4, 5, 7, 11 to 14 are above 95%, at locations 6, 8 and 10 are above 90%, at location 3 is above 86% and at locations 2 and 9 are insignificant.

Figure 6. First EOF mode of monthly averaged (a) SWH (92%) and (b) wind speed (70%) of NIO. (c) PC1 of SWH and wind speed from 1979 to 2012. (d) The climatology of wind speed square (m^2/s^2) of NIO. (e) First mode EOF of monthly anomaly of SWH (51%) and (f) PC1 of monthly anomaly of SWH and wind speed.

Figure 7. Time series plot of monsoon mean SWH and wind speed within the box 10° N to 15° N and 60° E to 65° E at central AS and monthly average rainfall data during June to September in central west coast of India

Figure 8. Wavelet analysis of monthly PC1 of (a) SWH, (b) wind speed. Monthly average rainfall data in (c) central west coast of India and (d) all over the Indian mainland. Oscillations with period one year and less than one year are removed from all data using low pass filter.

Figure 9. Wavelet coherence of spatially and monthly averaged SWH within the box 10° N to 15° N and 60° E to 65° E at western and central AS with monthly average rainfall data in central west coast of India.

Figure 10. a) Number of cyclones and b) maximum cyclone intensity in NIO from 1979 to 2012

Figure 11. a) Very severe cyclone tracks b) time series significant wave height at the maximum cyclone intensified location c) observed significant wave height during peak events d) observed wind speed at the peak events

Table 1. Details of the cyclone dates and the location of maximum intensity

Number	Date of occurrence (start and end date)	Maximum cyclone speed (Knots)	Latitude (Deg)	Longitude (Deg)
1	06/16/1979-06/20/1979	50	18.2	62.0
2	09/16/1979-09/25/1979	55	19.5	63.5
3	09/08/1983-10/08/1983	45	20.8	60.2
4	04/06/1987-12/06/1987	50	16.1	63.5
5	07/06/1989-06/13/1989	35	21.4	65.7
6	09/29/1992-04/10/1992	55	17.9	61.3
7	05/11/1993-11/16/1993	80	20.9	64.2
8	05/06/1994-09/06/1994	45	18.9	62.9
9	11/10/1995-10/18/1995	50	17.1	68.3
10	09/06/1996-12/06/1996	40	18.6	58.7
11	09/28/1998-01/10/1998	35	18.2	65.7
12	11/12/1998-12/17/1998	65	16.8	65.8
13	09/24/2001-09/28/2001	35	18.2	66.6
14	05/31/2007-08/06/2007	145	19.9	64.1
15	05/30/2010-07/06/2010	125	18.2	60
16	11/25/2011-01/12/2011	35	14.6	68.7

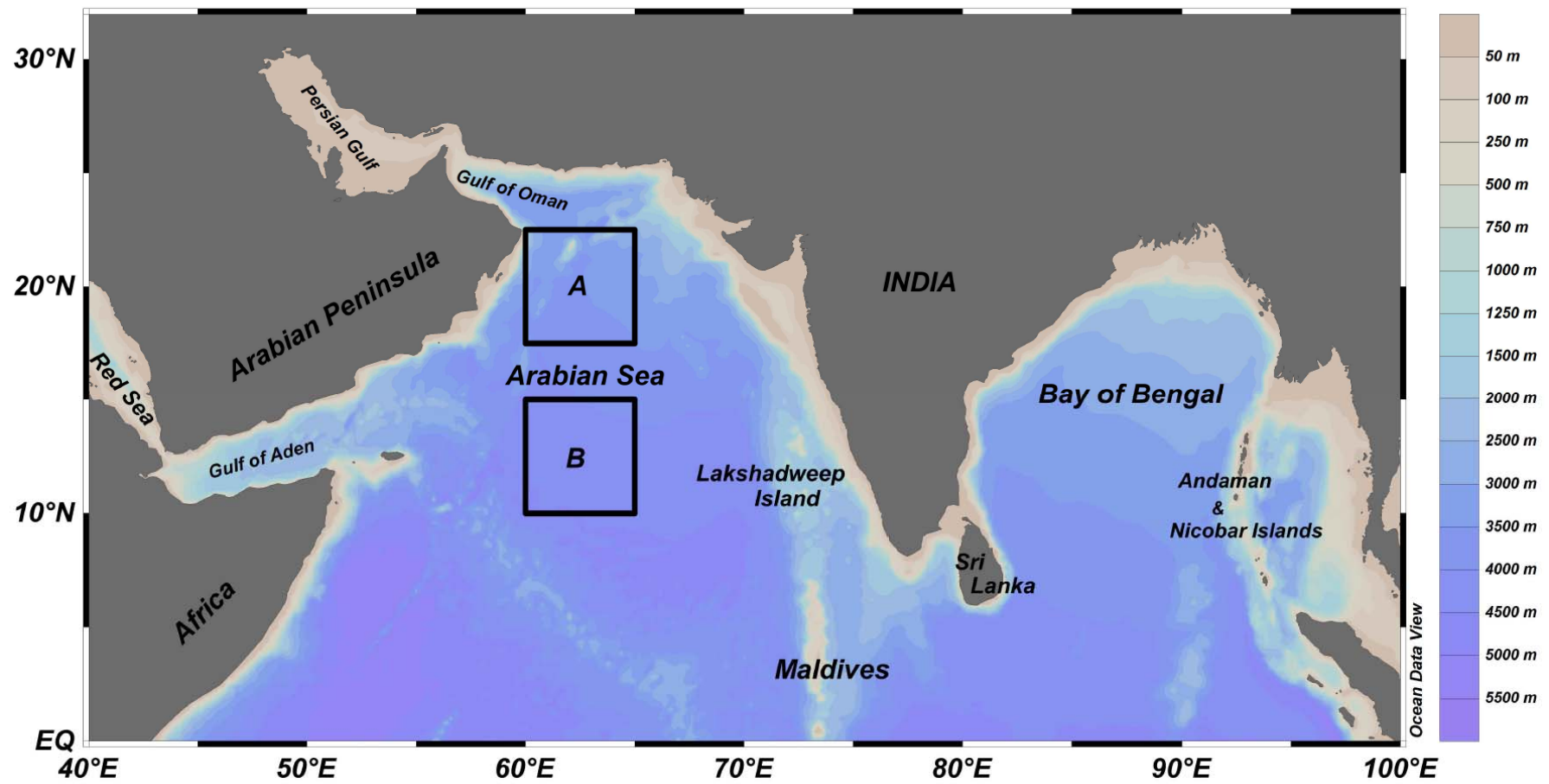


Figure 1. The map showing the area studied (North Indian Ocean). The shadings are the depth in m. Map is plotted using ocean data viewer. The area ($17.5\text{-}22.5^{\circ}\text{ N}$ and $60\text{-}65^{\circ}\text{ E}$) to analyze the link between the severe cyclone events and SWH is shown as A. The area in AS ($10\text{-}15^{\circ}\text{ N}$ and $60\text{-}65^{\circ}\text{ E}$) used to study the phase relation between the SWH and rainfall in central west coast of India is shown as B.

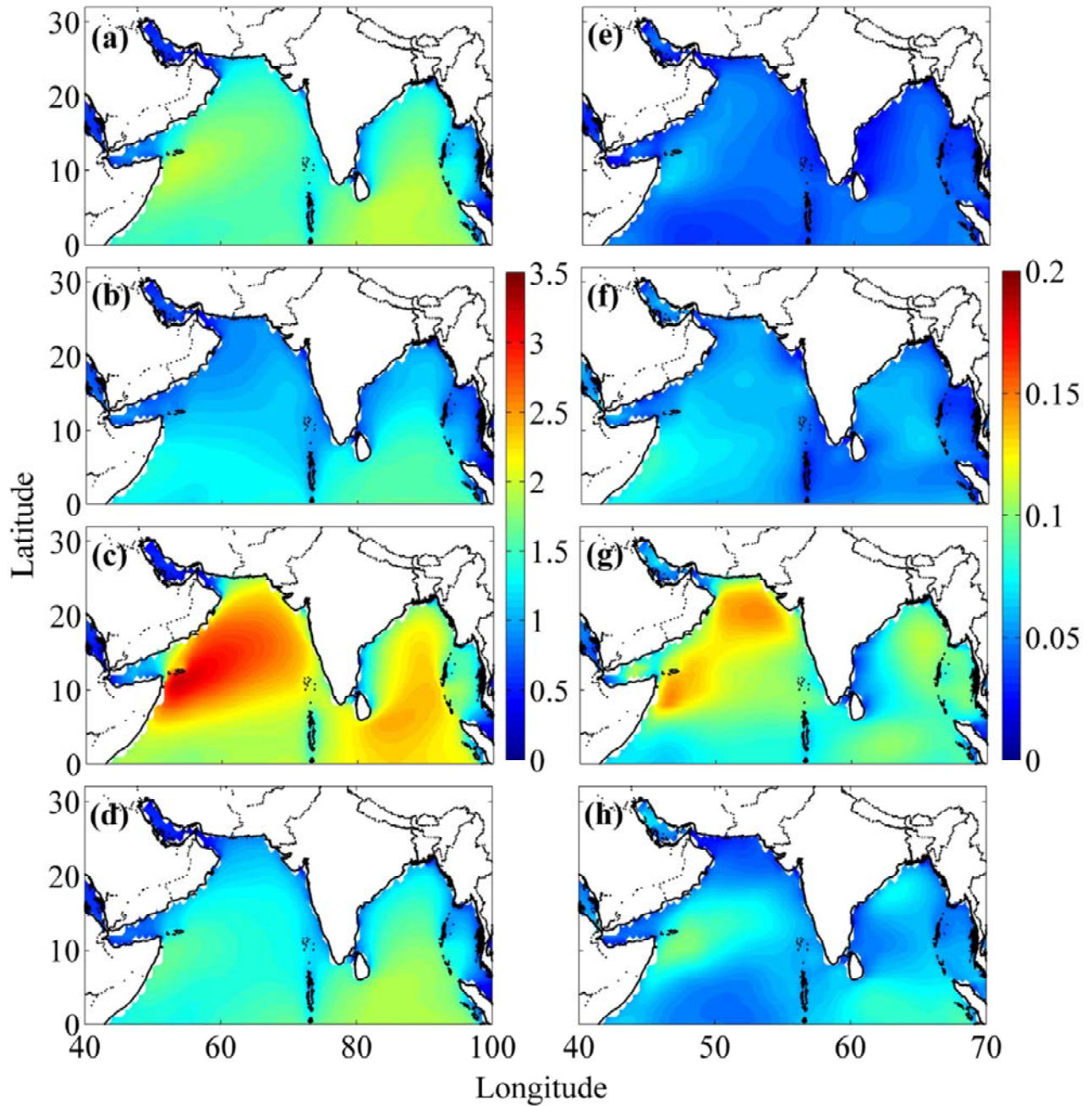


Figure 2. North Indian Ocean wave climatology based on data from 1979 to 2012. Left panel shows the mean significant wave height a) annual, b) pre-monsoon, c) monsoon and d) post-monsoon. Right panel shows the standard deviation of significant wave height in NIO; e) annual, f) pre-monsoon, g) monsoon and h) post-monsoon. All the values are in meter.

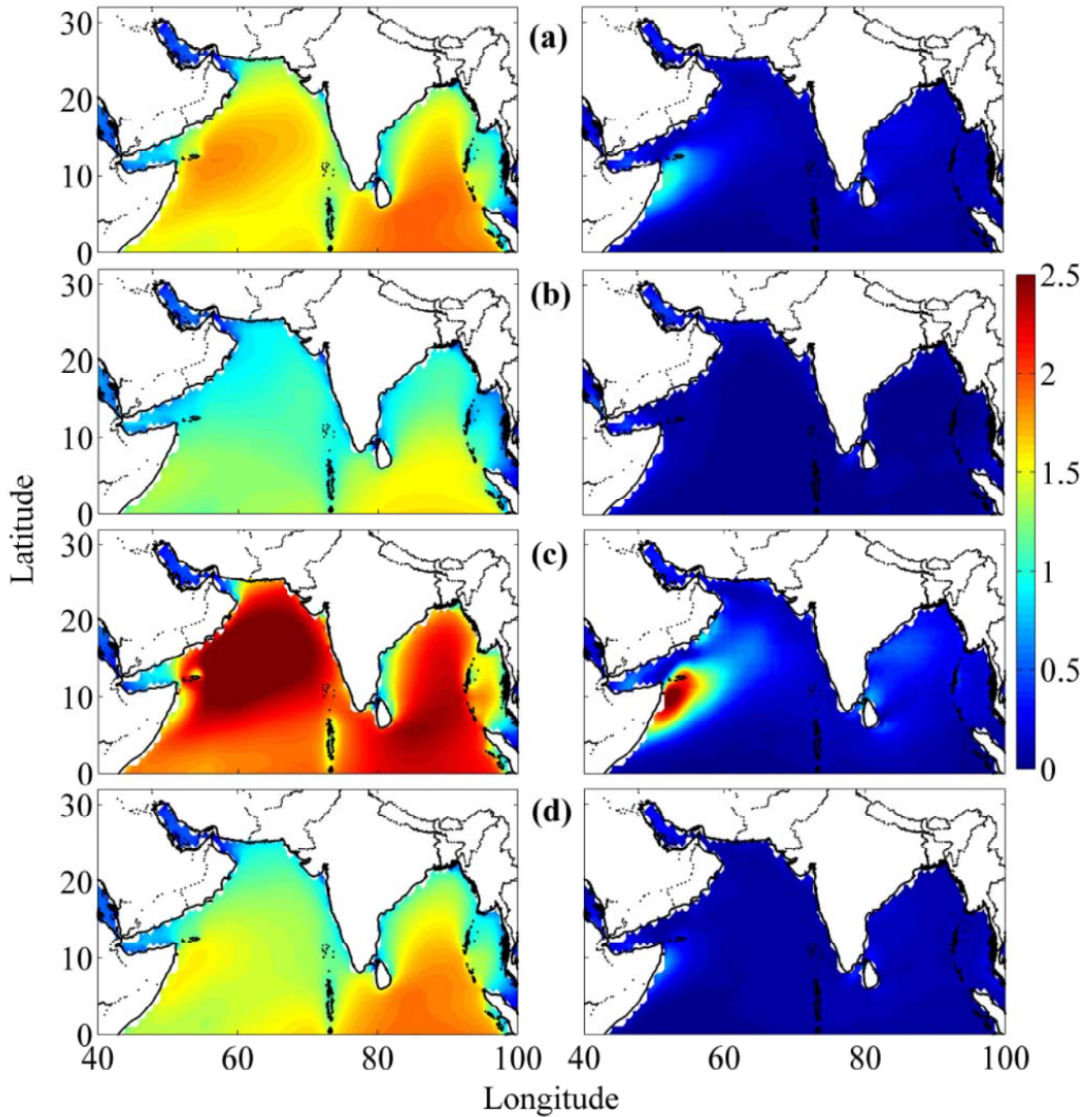


Figure 3. Mean swell (left panel) and wind sea (right panel) height in NIO by wave energy statistical method (a. Annual, b. Pre-monsoon (FMAM), c. Monsoon (JJAS) and d. Post-monsoon (ONDJ). All the values are in meter.

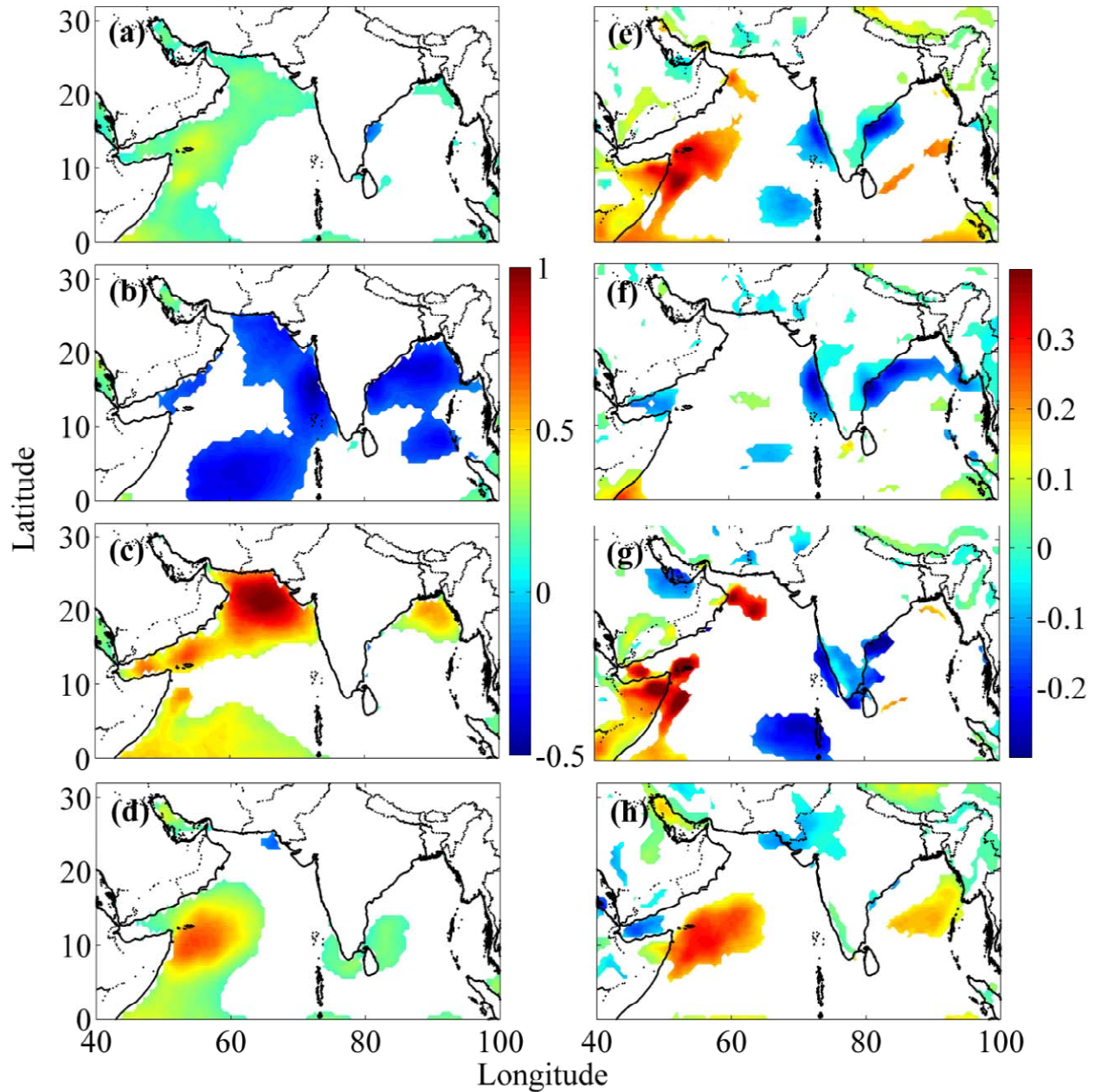


Figure 4. Left panel shows the trend of significant wave height (cm yr^{-1}) (a. Annual, b. Pre-monsoon, c. Monsoon, d. Post-monsoon). Right panel shows the trend of wind speed ($\text{m s}^{-1} \text{yr}^{-1}$) (e. Annual, f. Pre-monsoon, g. Monsoon, h. Post-monsoon). White patches in oceans indicate values which fail to achieve statistical significance. Statistical significance more than 90% only is presented in this figure.

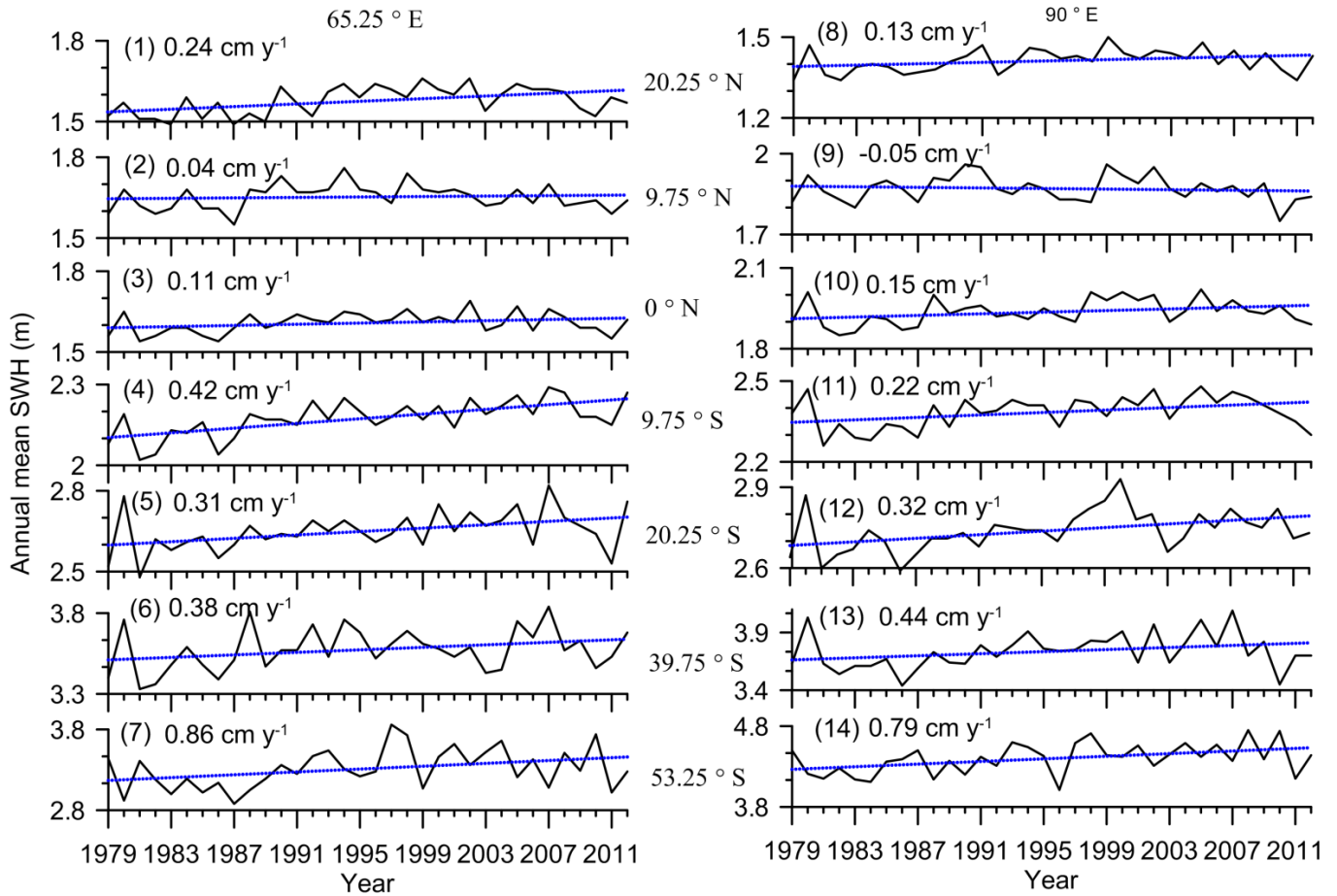


Figure 5. Trend of annual mean SWH along two transects in Indian Ocean. The left panel is along 65.25 °E and the right panel is along 90 °E. Statistical significance levels of the trends at locations 1, 4, 5, 7, 11 to 14 are above 95%, at locations 6, 8 and 10 are above 90%, at location 3 is above 86% and at locations 2 and 9 are insignificant.

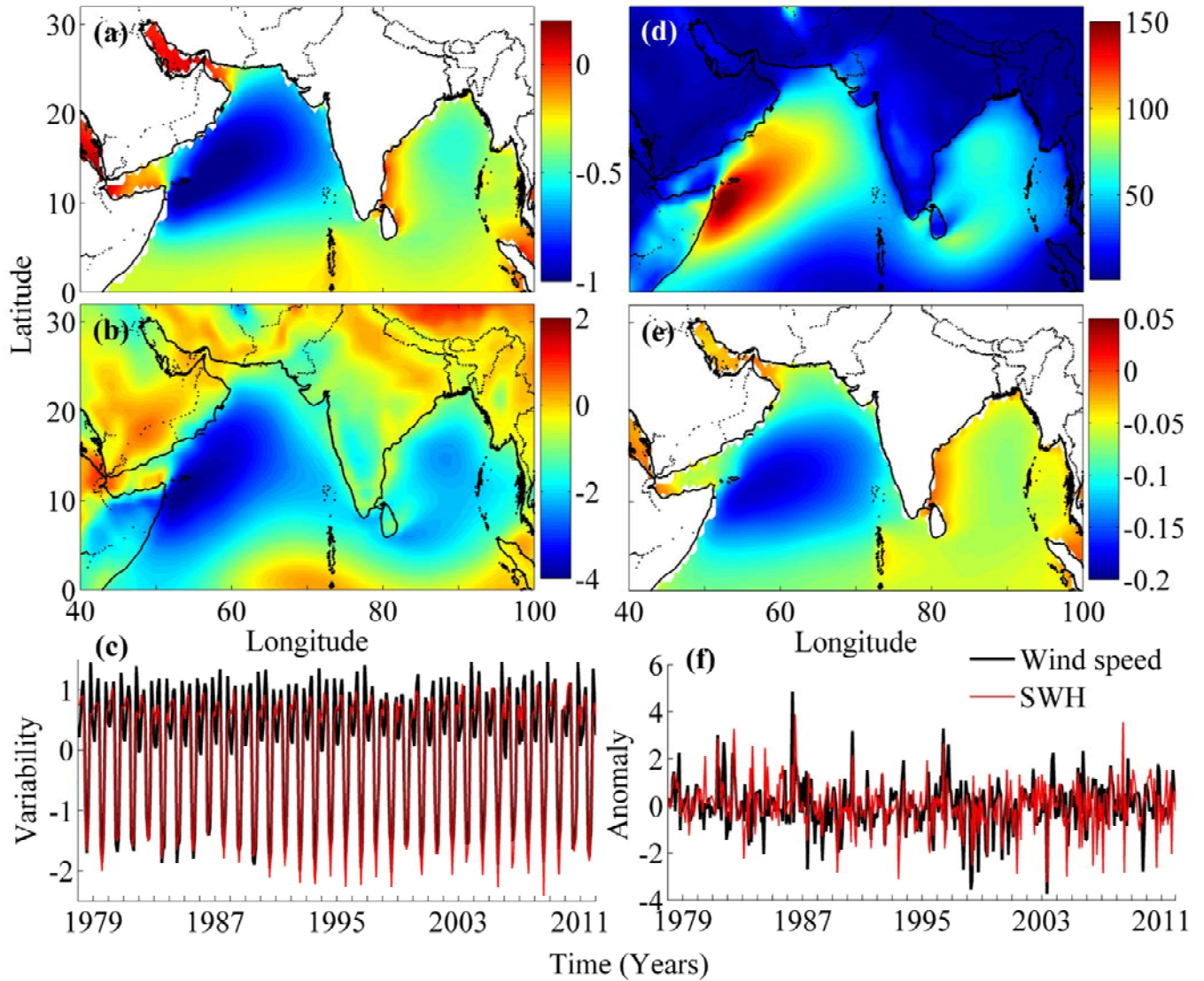


Figure 6. First EOF mode of monthly averaged (a) SWH (92%) and (b) wind speed (70%) of NIO. (c) PC1 of SWH and wind speed from 1979 to 2012. (d) The climatology of wind speed square (m^2/s^2) of NIO. (e) First mode EOF of monthly anomaly of SWH (51%) and (f) PC1 of monthly anomaly of SWH and wind speed.

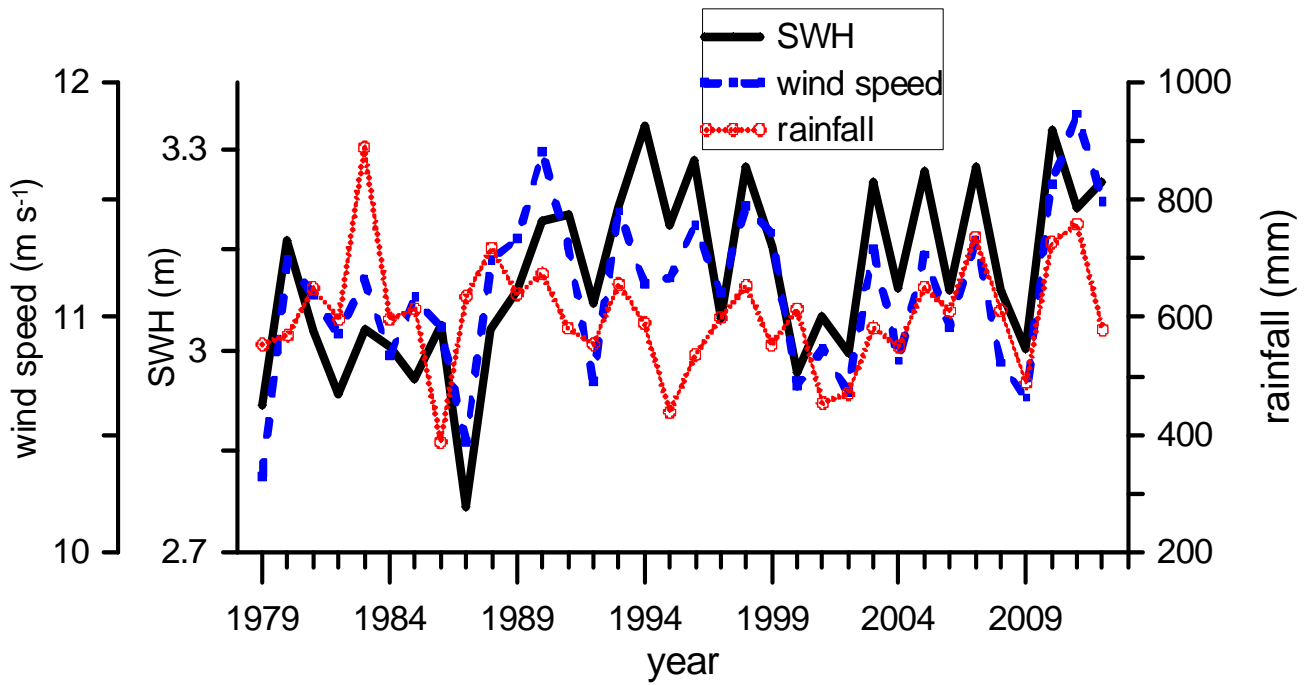


Figure 7. Time series plot of monsoon mean SWH and wind speed within the box 10°N to 15°N and 60°E to 65°E at central AS and monthly average rainfall data during June to September in central west coast of India.

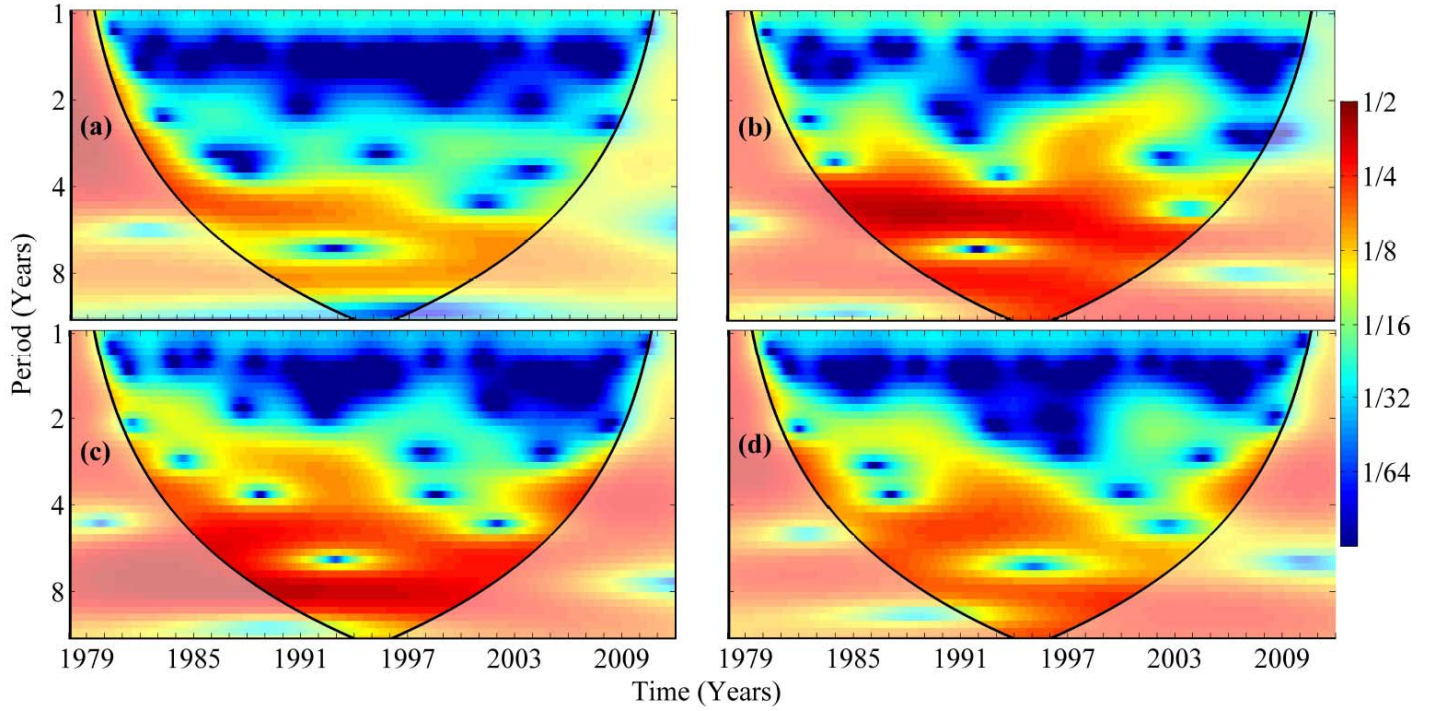


Figure 8. Wavelet analysis of monthly PC1 of (a) SWH, (b) wind speed. Monthly average rainfall data in (c) central west coast of India and (d) all over the Indian mainland. Oscillations with period one year and less than one year are removed from all data using low pass filter.

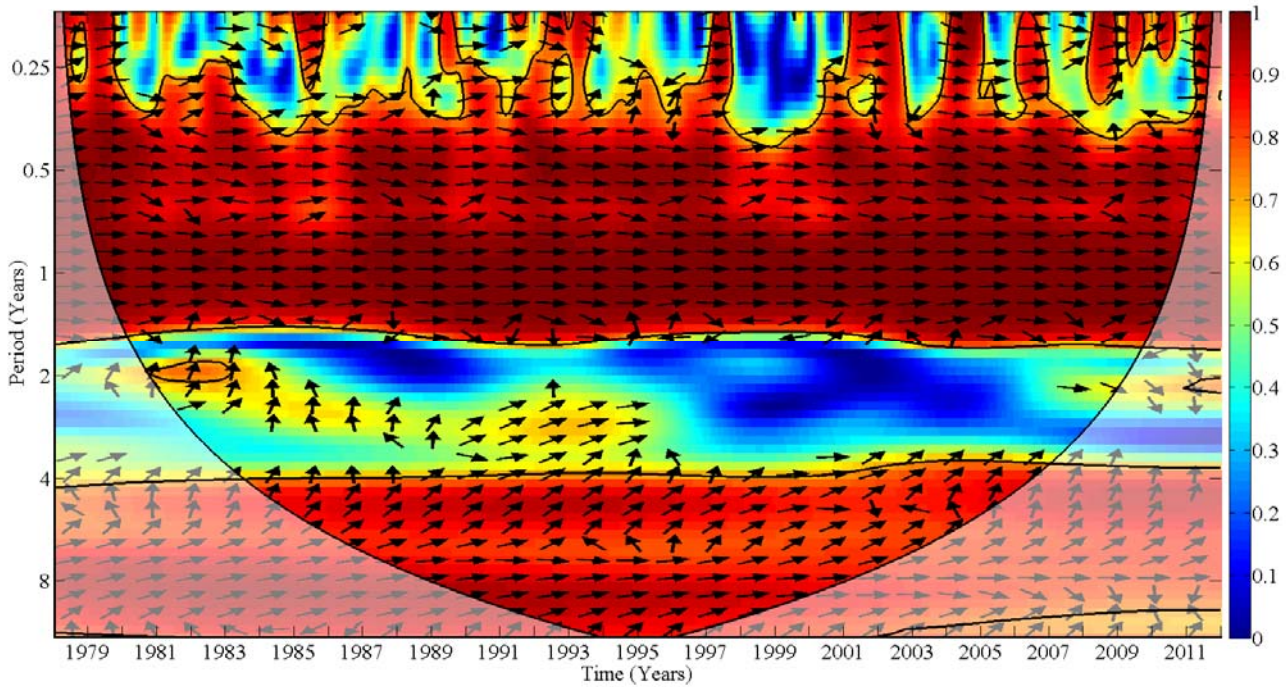


Figure 9. Wavelet coherence of spatially and monthly averaged SWH within the box 10°N to 15°N and 60°E to 65°E at central AS with monthly average rainfall data in central west coast of India.

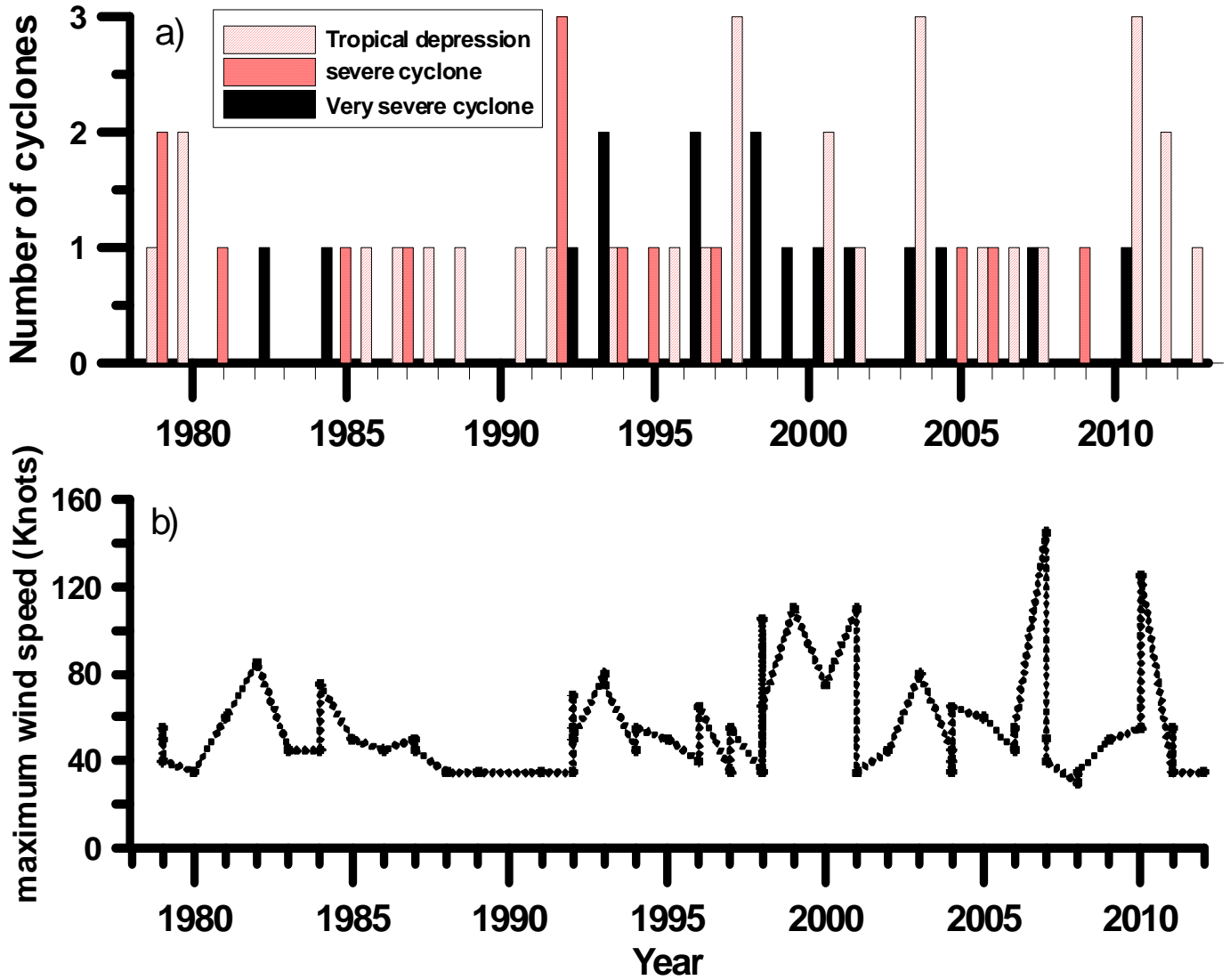


Figure 10. a) Number of cyclones and b) maximum cyclone intensity in NIO from 1979 to 2012

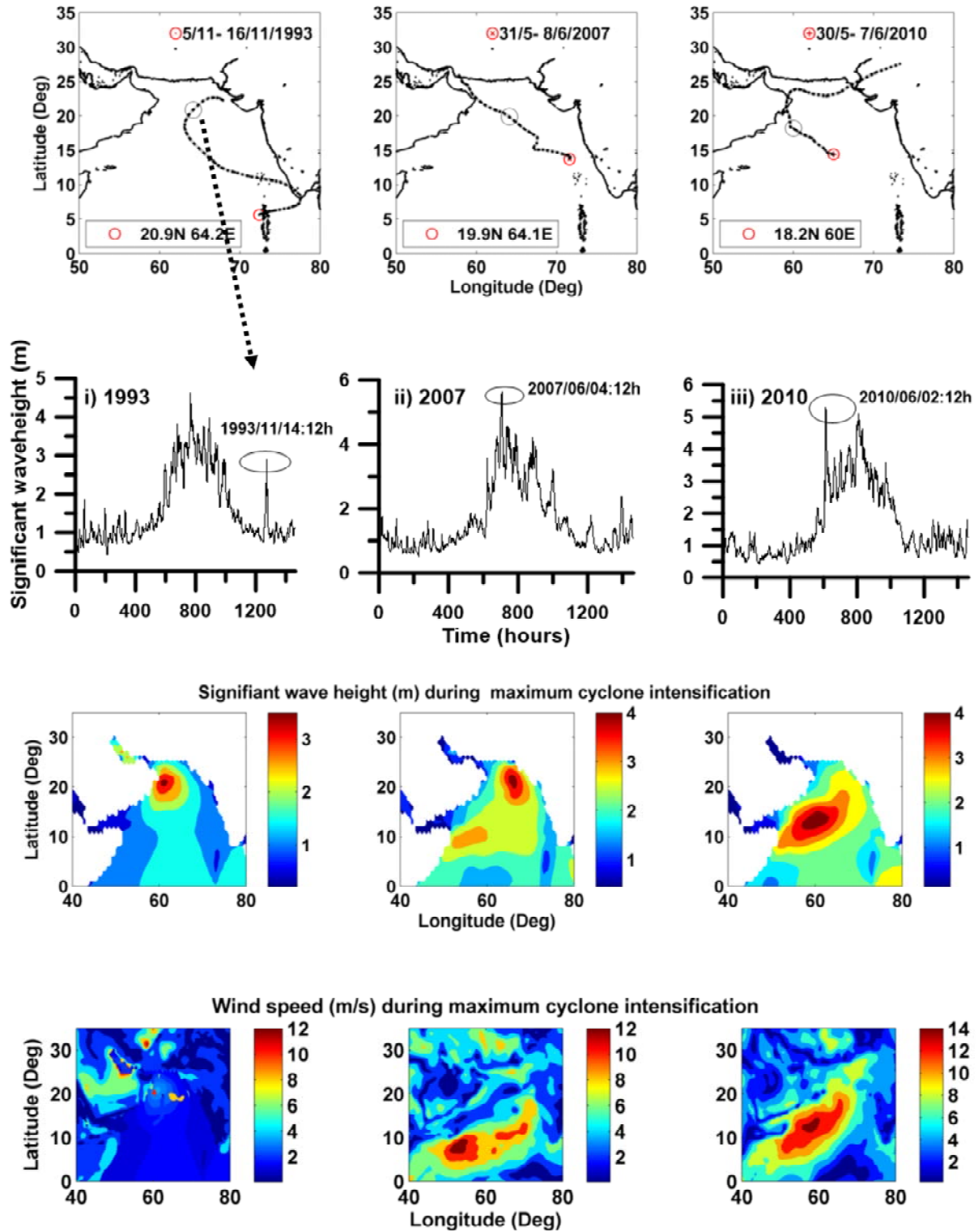


Figure 11.a) Very severe cyclone tracks b) time series significant wave height at the maximum cyclone intensified location c) observed significant wave height during peak events d) observed wind speed at the peak events